Microglia inhibit photoreceptor cell death and regulate immune cell infiltration in response to retinal detachment

Yoko Okunuki[a], Ryo Mukai[a], Elizabeth A. Pearsall[a], Garrett Klokman[a], Deeba Husain[a], Dong-Ho Park[a], Ekaterina Korobkina[b], Howard L. Weiner[c,d], Oleg Butovsky[c,d], Bruce R. Ksander[b], Joan W. Miller[a], and Kip M. Connor[a,1]

[a]Angiogenesis Laboratory, Department of Ophthalmology, Massachusetts Eye and Ear, Harvard Medical School, Boston, MA 02114; [b]Schepens Eye Research Institute, Massachusetts Eye and Ear, Department of Ophthalmology, Harvard Medical School, Boston, MA 02114; [c]Ann Romney Center for Neurologic Diseases, Department of Neurology, Brigham and Women's Hospital, Harvard Medical School, Boston, MA 02115; and [d]Evergrande Center for Immunologic Diseases, Brigham and Women's Hospital, Harvard Medical School, Boston, MA 02115

Edited by Gerard A. Lutty, Johns Hopkins School of Medicine, Baltimore, MD, and accepted by Editorial Board Member Jeremy Nathans May 21, 2018 (received for review November 21, 2017)

Retinal detachment (RD) is a sight-threatening complication common in many highly prevalent retinal disorders. RD rapidly leads to photoreceptor cell death beginning within 12 h following detachment. In patients with sustained RD, progressive visual decline due to photoreceptor cell death is common, leading to significant and permanent loss of vision. Microglia are the resident immune cells of the central nervous system, including the retina, and function in the homeostatic maintenance of the neuro-retinal microenvironment. It is known that microglia become activated and change their morphology in retinal diseases. However, the function of activated microglia in RD is incompletely understood, in part because of the lack of microglia-specific markers. Here, using the newly identified microglia marker P2ry12 and microglial depletion strategies, we demonstrate that retinal microglia are rapidly activated in response to RD and migrate into the injured area within 24 h post-RD, where they closely associate with infiltrating macrophages, a population distinct from microglia. Once in the injured photoreceptor layer, activated microglia can be observed to contain autofluorescence within their cell bodies, suggesting they function to phagocytose injured or dying photoreceptors. Depletion of retinal microglia results in increased disease severity and inhibition of macrophage infiltration, suggesting that microglia are involved in regulating neuroinflammation in the retina. Our work identifies that microglia mediate photoreceptor survival in RD and suggests that this effect may be due to microglial regulation of immune cells and photoreceptor phagocytosis.

microglia | retinal detachment | photoreceptor cell death | phagocytosis | macrophages

Retinal detachment (RD) is a sight-threatening complication of a variety of common retinal disorders including rhegmatogenous RD (1), neovascular age-related macular degeneration (2), and diabetic retinopathy (3). In patients with sustained RD, progressive visual decline due to photoreceptor cell death is common (4) and leads to significant and permanent vision loss (1, 5). Photoreceptor cell death occurs when photoreceptor outer segments are physically separated from the underlying retinal pigment epithelium (RPE) and choroidal vasculature, which provide metabolic support and oxygen to the outer layers of the retina (6, 7). While numerous pathological changes occur in the detached retina (8), studies using patient samples and animal models have shown that photoreceptor cell death is induced as early as 12 h after RD (4, 9). In the pathogenesis of RD, several inflammatory factors have been associated with the progression of photoreceptor cell death including MCP-1, TNF-α, and IL-1β (10–13). Macrophage/microglia infiltration into the retina after RD was previously thought to contribute to RD-induced photoreceptor apoptosis (9).

Microglia are resident immune cells of the CNS/retina, and function in the homeostatic maintenance of the neuro-retinal microenvironment (14). In healthy eyes, microglia typically have a highly ramified morphology, and their cell bodies are located in the inner retina, including the ganglion cell layer, the inner plexiform layer (IPL), and the outer plexiform layer (OPL) of the retina, and are not present in the photoreceptor cell layer (15). Previous studies have demonstrated that microglia are activated during retinal disease processes including glaucoma (16), retinitis pigmentosa (17), age-related macular degeneration (18), retinopathies (19–21), and RD (11, 15, 22, 23). Once microglia are activated, they become increasingly mobile, their horizontal processes shrink, and their morphology becomes amoeboid in nature. Activated microglia perform multiple functions such as phagocytosis, antigen presentation, and production of inflammatory factors, which can be either beneficial or harmful to the affected tissue (24, 25). Multiple studies have suggested that activated microglia promote neuronal cell death in both the retina and the brain (11, 26–28), including animal models of RD and inherited retinal degeneration, in which photoreceptor cell death is a key process in the pathogenesis (23, 29). It has been reported that microglia phagocytize live photoreceptor cells and

Significance

Photoreceptor cell death resulting from retinal detachment (RD) causes significant visual loss. While the immune system is activated during RD, its role is still unclear. Microglia are resident immune cells in the retina and are thought to be either protective or deleterious in response to neuronal injury, suggesting context-dependent effects. Here, we demonstrate that microglia limit retinal damage during acute injury, since microglial ablation led to increased photoreceptor death. Microglial morphological–activation changes triggered their migration into injured tissue where they formed intimate connections with infiltrating immune cells and phagocytized injured photoreceptors. These findings provide insight into the microglial response and function during RD, indicating microglia promote photoreceptor survival during acute phase injury by removing potentially damaging cell debris.

Author contributions: Y.O. and K.M.C. designed research; Y.O., E.A.P., G.K., and E.K. performed research; Y.O., R.M., D.H., D.-H.P., H.L.W., O.B., B.R.K., J.W.M., and K.M.C. analyzed data; and Y.O. and K.M.C. wrote the paper.

The authors declare no conflict of interest.

This article is a PNAS Direct Submission. G.A.L. is a guest editor invited by the Editorial Board.

This open access article is distributed under Creative Commons Attribution-NonCommercial-NoDerivatives License 4.0 (CC BY-NC-ND).

[1]To whom correspondence should be addressed. Email: kip_connor@meei.harvard.edu.

This article contains supporting information online at www.pnas.org/lookup/suppl/doi:10.1073/pnas.1719601115/-/DCSupplemental.

Published online June 18, 2018.

www.pnas.org/cgi/doi/10.1073/pnas.1719601115

Downloaded at Palestinian Territory, occupied on December 1, 2021

worsen photoreceptor loss in retinal degeneration (29). In contrast, other studies have reported a protective function for activated microglia in ischemic brain injury, in which neuronal cell death is the main cause of pathogenesis (30, 31). However, whether microglia activity affects photoreceptor cell death in RD has not been clearly investigated.

The role and function of microglia in disease progression is not well understood due to the multiple phenotypes and/or different stages of activation of microglia that are associated with either harmful or beneficial effects during disease pathogenesis. Predominantly, investigators have struggled to understand how microglia are related to monocytes/macrophage populations during neuroinflammation. This is due in part to the lack of microglial-specific markers. The most commonly used markers in prior microglial studies are CX3CR1, CD11b, and Iba1 (32–34), which are also expressed in other types of immune cells such as monocytes and macrophages (35, 36). Thus, distinguishing microglia from other infiltrating immune cells is not possible using these markers, especially in the context of disease or injury, where inflammation is present. Previous research from our laboratory demonstrated that macrophages/microglia were observed in the subretinal space after RD (9, 13). We hypothesized that these cells contributed to local inflammation and affected photoreceptor cell death. However, given our reagents at the time, we were unable to elucidate the differential role of macrophages and microglia and their respective effects on photoreceptor cell death.

P2ry12 was previously shown to regulate microglial activation (37) and has recently been identified as a microglia-specific marker that is not expressed by monocytes or macrophages (35). In this study, we used an antibody against P2ry12, which allowed us to distinguish microglia from other types of immune cells during RD-induced inflammation. We first observed the dynamic morphological changes of microglia in RD, acquiring images that clearly depict microglia interacting with infiltrating macrophages and phagocytized photoreceptors. To directly assess the role of microglia in RD, we depleted microglia and assessed the severity of neurodegeneration in response to RD. Our results suggest that microglia inhibit photoreceptor cell death in acute RD and contribute to macrophage infiltration and photoreceptor phagocytosis.

Results

Longitudinal Assessment of Morphological Changes in Microglia Following RD. To define the activation of microglia in response to RD, we first examined the morphological changes microglia undergo in response to RD. We induced RD in mice and isolated retinas for whole-mount immunohistochemistry (IHC) at 1, 3, 6, 12, and 24 h after RD induction. Retinas were stained for the microglial-specific marker P2ry12. Isolectin GS-B4 (lectin) was used to label vessels to orientate microglia within the retina as well as to identify possible infiltrating immune cells. The entire retinal thickness of each detached area was scanned by confocal microscopy, and 3D reconstructions were performed using the software platform Amira (38). Untreated eyes served as a baseline (0 h). The superior orthogonal views of 3D-constructed retinal images illustrate that microglia are evenly distributed in the normal retina (Fig. 1). Post detachment, microglia begin to condense and migrate to the injured area, which is most prominent at 24 h post-RD (Fig. 1 and *SI Appendix*, Fig. S1*A*). When microglia in the detached area were focally examined by whole-mount IHC, microglial density was reduced in as little as 1 h post-RD ($P < 0.05$), reflecting microglial condensation and migration to the injured area (*SI Appendix*, Fig. S1 *A* and *B*). This condensation of the microglial cell body increased as disease progression occurred (24 h post-RD, $P < 0.0001$) (*SI Appendix*, Fig. S1 *A* and *B*). The number of microglia in the upper retina was significantly reduced at 24 h ($P < 0.001$) (*SI Appendix*, Fig. S1 *A* and *C*), a reflection of their migration into the photoreceptor cell layer and subretinal space in the region of injury (see *SI Appendix*, Fig. S13, which is described below). To determine if microglial cell numbers are stable throughout the disease course, we used flow cytometry with a marker that has been reported to be microglia specific, Fc-receptor like-S, scavenger receptor (Fcrls) (35), and quantified the number of microglia in the entire retina through disease progression. We found that Fcrls^{+} microglial numbers in whole-retinal suspensions were unchanged in response to RD (*SI Appendix*, Fig. S2). The 3D-constructed cross-sectional views of the retina clearly define the distribution of microglia. Before RD (0 h) microglia are located in the OPL, the IPL, and the ganglion cell layer and microglial processes or cell bodies are not present in the outer nuclear layer (ONL, the photoreceptor cell layer) (Fig. 2*A*). Microglia contain highly ramified processes parallel to the retinal

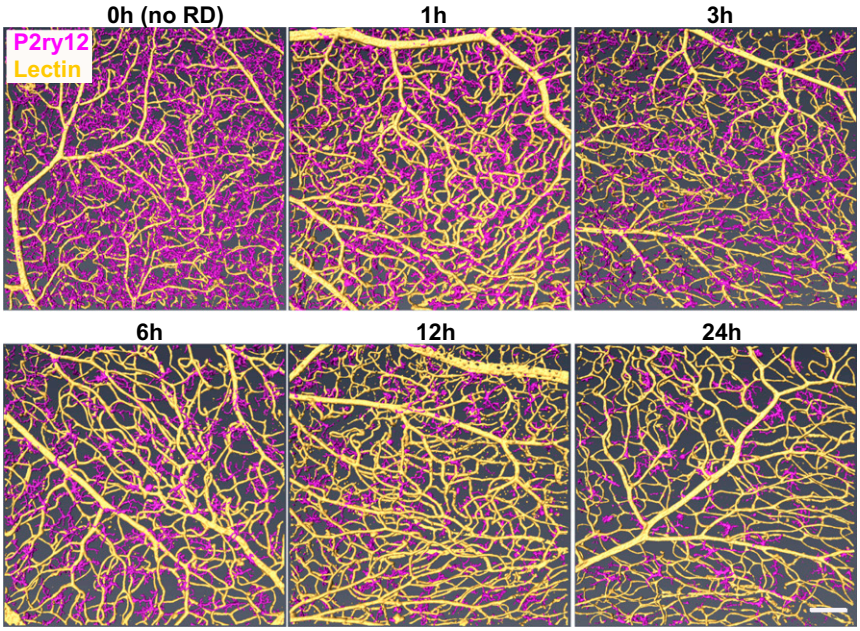

Fig. 1. Time-course images of the top view 3D-constructed retinas after RD. Retinas at various time points after detachment were whole-mount stained with anti-P2ry12 Ab (magenta) and lectin (yellow). Confocal images of the entire retinal thickness around the peak of RD were taken by a 20× lens and were 3D reconstructed using Amira software. At least six eyes were examined for each time point. (Scale bar: 100 μm.)

Downloaded at Palestinian Territory, occupied on December 1, 2021

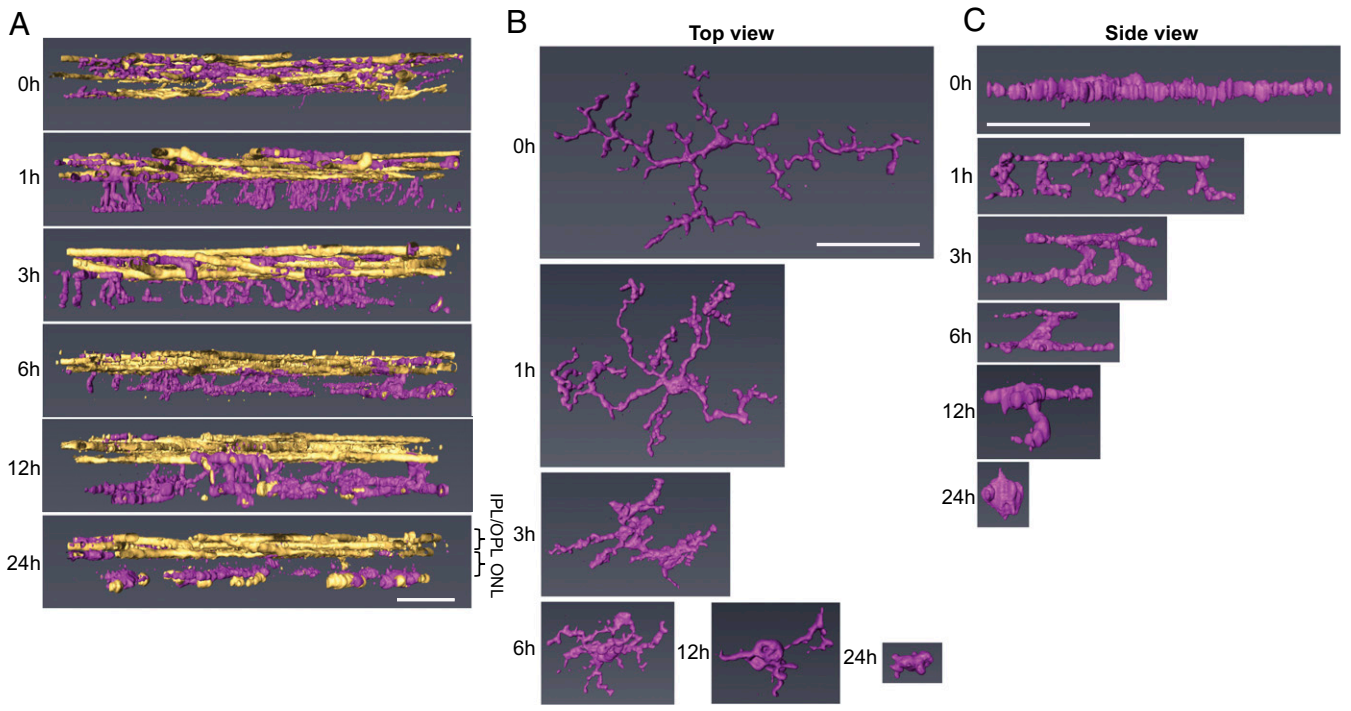

Fig. 2. Microglia change location and morphology within 24 h post-RD. Retinas at various time points after detachment were whole-mount stained with anti-P2ry12 Ab (magenta) and lectin (yellow). The confocal images around the peak of RD were taken by a 63× lens, and the images were 3D-reconstructed using Amira software. (*A*) The side view of the retinas shows the time-course change of microglia location and their processes in the ONL. (*B* and *C*) Top (*B*) and side (*C*) views of magnified images of a single microglia from each time point show the time-course change in shape and size. At least six eyes were examined for each time point. (Scale bars, 50 μm.)

vasculature in normal retinas (Fig. 2 *B* and *C*). In contrast, following RD, microglia become dynamic and migrate rapidly into the injured outer retina (Fig. 2*A* and *SI Appendix*, Fig. S3). Microglia rapidly extend their processes into the injured area in as little as 1 h post-RD; they then migrate to the outer retina while condensing their processes (Fig. 2). At 24 h post-RD, many of the microglial cell bodies in the detached area are located in the outermost layer of the retina. During this phase microglia take on a variety of morphological features suggesting differing levels of activation and potentially differential functions. A number of microglia in the injured photoreceptor layer demonstrate an amoeboid morphology (Fig. 2*A* and *SI Appendix*, Fig. S3), a microglial phenotype that is associated with an activated state (39). These results illustrate that, in response to RD injury, retinal microglia become activated within 24 h and migrate into the injured photoreceptor layer.

Depletion of Microglia in RD. Microglia are extremely dynamic in their morphology and are able to migrate rapidly into injured areas of the retina following RD. However, their function in RD injury remains unclear. It has been suggested that infiltrating macrophages and/or microglia contribute to photoreceptor cell death, the key pathology of RD (12, 13). However, the role of microglia in acute RD disease progression is still unclear. To begin to address this, we first depleted retinal microglia utilizing a transgenic (TG) approach and evaluated photoreceptor cell death in microglia-depleted animals. *Cx3cr1*^{CreER} mice, which express a Cre-ER fusion protein from endogenous CX3CR1 promoter enhancer elements (40), were crossed to B6-iDTR mice, which contain a flox-STOP-flox diphtheria toxin receptor (DTR) in the ROSA26 locus (41). In subsequent offspring, Cre recombinase activation under the control of the *Cx3cr1* promoter can be induced by tamoxifen, leading to expression of the human DTR on CX3CR1-expressing cells, including microglia (36). In a normal retina, essentially all CX3CR1^{+} cells are microglia, and therefore tamoxifen administration will trigger expression of the DTR only in retinal microglia. Cells expressing the DTR undergo cell death in response to the administration of diphtheria toxin (DTX) in this TG mouse system, allowing microglial depletion by DTX administration (40). To induce DTR expression in this system, we induced activation of Cre recombinase in TG mice with five consecutive days of i.p. tamoxifen injections starting at 6 wk of age. Two weeks later, retinal microglia were depleted by introducing DTX via the anterior chamber (AC) (42) to locally deplete CX3CR1^{+} cells within the retina and to minimize the systemic effect of DTX-induced cell death in circulating CX3CR1^{+} cells.

Injection of DTX in tamoxifen-treated TG mice depleted 88.5% of retinal microglia in 48 h ($P < 0.0001$) (Fig. 3*A* and *SI Appendix*, Fig. S4). However, tamoxifen i.p. injection alone also suppressed the number of microglia by approximately 30% (Fig. 3*A*). These data are consistent with a report that described tamoxifen suppression of microglial viability in vitro (43). To investigate the effect of microglial depletion in photoreceptor cell death, we administered DTX (AC) 48 h before and at the time of RD induction. Photoreceptor cell death was assessed 24 h post-RD, the peak of cell death in this model (9). Photoreceptor cell death in DTX-injected mice was significantly increased compared with saline-injected control mice ($P < 0.05$) (Fig. 3*B*). This supports a role for retinal microglia in safeguarding photoreceptors from cell death in response to RD. ONL thickness evaluated at 24 h post-RD did not differ between retinas with and without microglia depletion in TG mice (*SI Appendix*, Fig. S5*A*), indicating that microglia depletion by DTX did not affect the total number of photoreceptor cells at this acute time point.

However, because approximately 11.5% of P2ry12^{+} microglia still remained after microglial deletion using this TG mouse system (Fig. 3*A*), we could not exclude the possibility that the remaining microglia contributed to this finding. Moreover, because CX3CR1

Downloaded at Palestinian Territory, occupied on December 1, 2021

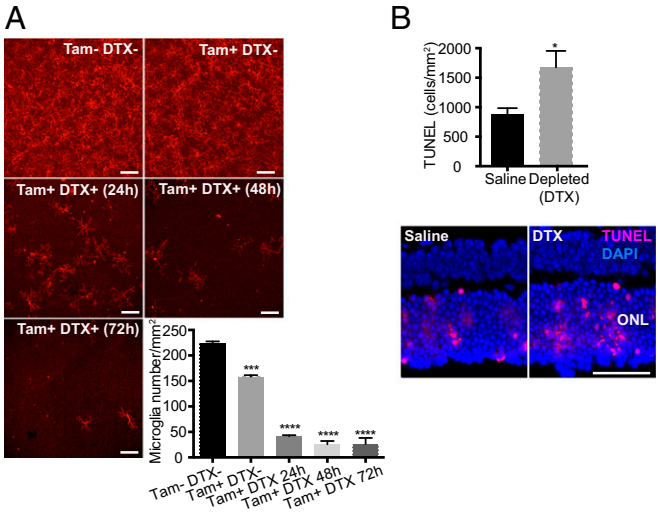

Fig. 3. Microglia depletion in TG (CX3CR1CreER × B6-iDTR) mice and photoreceptor cell death after RD. Retinal microglia were depleted in TG (CX3CR1CreER × B6-iDTR) mice, and photoreceptor cell death at 24 h after RD was evaluated by TUNEL staining. (*A*) Evaluation of microglia depletion in TG mice. The nondetached retinas of TG mice, with or without tamoxifen (Tam) injection (i.p.) and at various time points after DTX injection (AC), were stained for P2ry12. The whole-mount images of midperipheral retinas from each quadrant were taken by confocal microscopy using a 20× lens. Z-stack images of the entire thickness of the retina were created by ImageJ for microglia counting. Consequently, four images from one eye were used for the quantification of microglia number. (Scale bars: 100 μm.) $n = 3$–4. ***$P <$ 0.001; ****$P < 0.0001$, one-way ANOVA followed by Tukey's multiple comparison test. Representative entire retinal images are shown in *SI Appendix*, Fig. S3. (*B*) Quantification of TUNEL$^+$ cells at 24 h post-RD with or without microglia depletion in TG mice. $n = 6$. *$P < 0.05$, unpaired t test. Nuclei staining, DAPI. (Scale bar: 50 μm.) Data are expressed as mean ± SEM.

is not microglia specific, especially in the setting of inflammation, it is possible that targeting CX3CR1$^+$ cells led to the depletion of other populations such as infiltrating macrophages. Therefore, we next utilized a pharmacologic approach to deplete microglia by targeting colony-stimulating factor 1 receptor (CSF1R), a receptor required for microglia survival (44). We utilized an orally administered CSF1R antagonist, PLX5622, to deplete microglia. After 7 d of administration of PLX5622, formulated in chow (1,200 ppm), no microglia were detected in the retina (Fig. 4*A* and *SI Appendix*, Fig. S6).

We started the PLX5622 diet 7 d before RD induction and assessed photoreceptor cell death. At 24-h post-RD, retinas from PLX5622-fed mice had a significant increase in the number of TUNEL$^+$ cells in the ONL compared with retinas from mice receiving control diet ($P < 0.05$) (Fig. 4*B*). These results are consistent with the results from our microglia depletion study in TG mice (Fig. 3*B*), further confirming that microglia inhibit photoreceptor cell death in response to acute RD injury. ONL thickness evaluated at 24 h post-RD did not differ between retinas with and without microglia depletion with PLX5622 (*SI Appendix*, Fig. S5*B*), indicating that microglia depletion by PLX5622 did not affect the total number of photoreceptor cells at this acute time point. Retinal function evaluation by electroretinography (ERG) at 7 d post-RD did not show a difference between the RD retinas with and without microglia depletion by PLX5622 (*SI Appendix*, Fig. S7). Of note, the a- and b-wave amplitudes from human patients with total rhegmatogenous RD are almost nonrecordable (45); therefore these findings are not unexpected. Consequently, it is likely that recordings of full-field ERG in partial RD originate mostly from the nondetached retina, so any effects on photoreceptor survival in the detached retina would not be reflected in the ERG response. This point is further detailed in *Discussion*.

We next examined the relationship among microglia, photoreceptors, and TUNEL$^+$ nuclei by IHC to ensure that microglial death was completed before RD induction and did not affect TUNEL$^+$ cell numbers in PLX5622-treated mice with RD and that cell populations other than photoreceptor cells did not contribute to TUNEL$^+$ cell numbers. We first examined if PLX5622 affected the number of TUNEL$^+$ cells in naive/healthy retinas. Although TUNEL$^+$ cells were not observed in control retinas (*SI Appendix*, Fig. S8*A*), TUNEL$^+$ microglia were detected at early time points (day 1–2) of PLX5622 administration (*SI Appendix*, Fig. S8 *B* and *C*). After 7 d of PLX5622 administration, microglia were not observed, and there were no TUNEL$^+$ cells in the ONL (*SI Appendix*, Fig. S8*D*). This result confirms that microglia death is complete by day 7 of PLX5622 administration and does not affect the number of TUNEL$^+$ cells in PLX5622-treated RD mice. Complete depletion of microglia was also confirmed in PLX5622-treated RD mice (*SI Appendix*, Fig. S9), suggesting that dying microglia in PLX5622-treated retinas do not contribute to TUNEL$^+$ cells in the ONL.

Next we examined localization of TUNEL$^+$ nuclei within the cells of the ONL in association with a photoreceptor-specific cell marker, recoverin, which is a membrane protein. TUNEL$^+$ nuclei at 24 h post-RD with and without microglia depletion were located inside the staining of recoverin$^+$ cells, confirming that TUNEL$^+$ cells were photoreceptors (*SI Appendix*, Fig. S10). Together, these data confirm that the increase in TUNEL$^+$ cells in

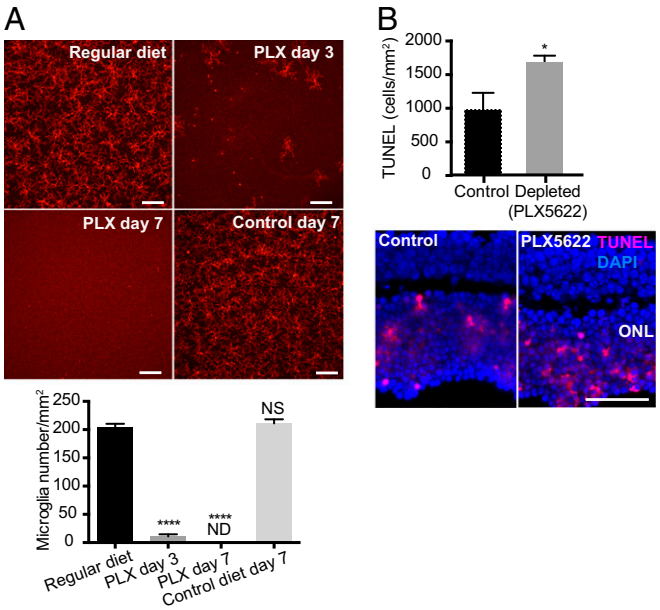

Fig. 4. Microglia depletion by PLX5622 and photoreceptor cell death after RD. Retinal microglia were depleted by PLX5622 in C57BL/6 mice, and photoreceptor cell death at 24 h post-RD was evaluated by TUNEL staining. (*A*) Evaluation of microglia depletion by PLX5622 in C57BL/6 mice. The nondetached retinas from mice given regular diet, control diet, and PLX5622 were stained for P2ry12. The whole-mount images of midperipheral retinas from each quadrant were taken by confocal microscopy using a 20× lens. Z-stack images of the entire thickness of the retina were created by ImageJ for microglia counting. Consequently, four images from one eye were used to calculate the number of microglia of the retina. (Scale bars: 100 μm.) $n = 3$–4. ****$P < 0.0001$, one-way ANOVA followed by Tukey's multiple comparison. ND, not detected; NS, not significant. Representative entire retinal images are shown in *SI Appendix*, Fig. S4. (*B*) Quantification of TUNEL$^+$ cells at 24 h post-RD with or without microglia depletion by PLX5622. $n = 6$. *$P < 0.05$, unpaired t test. Nuclei staining, DAPI. (Scale bar: 50 μm.) Data are expressed as mean ± SEM.

Downloaded at Palestinian Territory, occupied on December 1, 2021

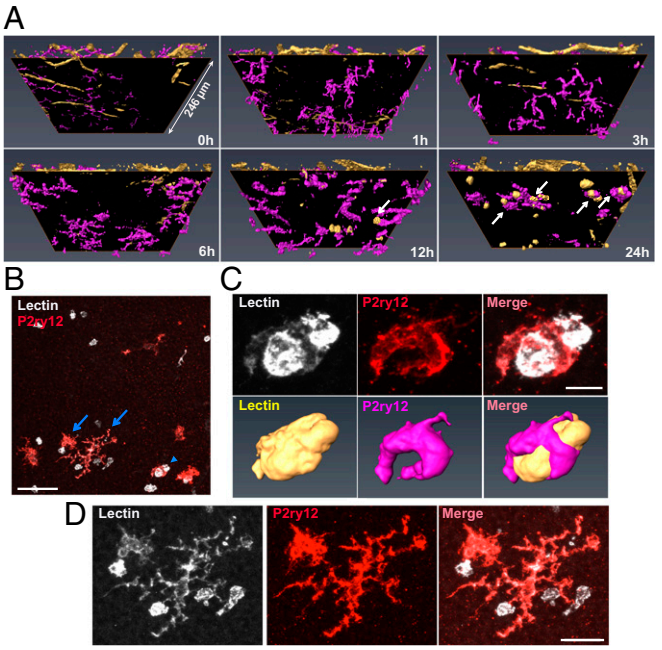

Fig. 5. Microglia localized in the ONL interact with lectin$^+$ cells. (*A*) The images used in Fig. 2*A* were turned 30° on the *x* axis. Black surfaces were inserted between the vessel layers and the ONL. The images under the surfaces show the ONL and the photoreceptor layer. Microglia interacting with lectin$^+$ cells at 12 and 24 h are indicated with arrows. One side of the retinal image is 246 μm. (*B*) A z-stack image of the ONL and the photoreceptor layer of Fig. 2 (24 h) was created using ImageJ. The arrowhead indicates the microglia magnified in *C*, and the arrows indicate the microglia in *D*. (*C*) The magnified z-stack images and the corresponding 3D-reconstructed images show that the microglia wraps around the lectin$^+$ cells. (*D*) Two other adjacent microglia are contacting lectin$^+$ cells. (Scale bar: 50 μm in *B*; 10 μm in *C*; 20 μm in *D*.)

RD following microglia depletion was due to increased photoreceptor cell death.

Microglial Association with Inflammatory Cells in the Photoreceptor Layer After RD. Our results illustrated that, following RD, microglia migrated rapidly into the photoreceptor layer. However, microglia are not the only population infiltrating into the subretina after RD injury. We observed lectin$^+$ cells infiltrating into the retina at 12 h post-RD, becoming more prominent at 24 h (Fig. 5*A*). This observation is consistent with our earlier studies in which CD11b$^+$ cells appeared in the subretina beginning at 12 h after RD (9). We next examined the characteristics of infiltrating inflammatory cells, as the infiltrating CD11b$^+$ subretinal cells could be either activated microglia or infiltrating macrophages (9, 11, 13, 23).

To observe the detail of lectin$^+$ cells in the photoreceptor layer, 3D orthogonal views from retinal whole mounts were constructed with a view projected from the subretina in lectin- and P2ry12-labeled samples (Fig. 5*A*). The upper retinal layers were segmented by a black surface so that only the ONL and the photoreceptor inner and outer segment layers were observed. Interestingly, some of the microglia appeared to interact directly with lectin$^+$ cells, which were observed at 12 and 24 h post-RD (Fig. 5 *A* and *B*). The magnified z-stack images and the 3D-constructed images of microglia show that the P2ry12$^+$ microglia were wrapping around (Fig. 5*C*) and interacting with lectin$^+$ cells (Fig. 5*D*), suggesting that a subset of microglia actively phagocytize infiltrating lectin$^+$ cells and communicate with infiltrating cells via their processes. The 360° movie images of these microglia (Movies S1 and S2) more clearly demonstrate that microglia interact directly with infiltrating lectin$^+$ cells. These images strongly suggest that P2ry12$^+$ microglia and infiltrating lectin$^+$ immune cells are distinct populations. However, microglia are weakly positive for lectin staining, and this staining is relatively nonspecific for immune cell types (Fig. 5 *C* and *D*). Given this, we next performed a more detailed characterization of lectin$^+$ cells utilizing reported microglia/macrophage markers (46). IHC for CD11b clearly stained lectin$^+$ cells, while P2ry12$^+$ ramified microglia had only faint CD11b reactivity (Fig. 6*A*). On the other hand, anti-F4/80 IHC did not stain infiltrating lectin$^+$ cells but appeared to stain activated P2ry12$^+$ microglia (Fig. 6*B*). 3D-reconstructed images clearly show microglia directly interacting with CD11b$^+$ macrophages (Movie S3). In addition, a number of lectin$^+$ infiltrating immune cells were CX3CR1$^-$ when GFP signal was examined in retinas from CX3CR1$^{+/GFP}$ mice (Fig. 6*C*), supporting previous work identifying these cells as activated monocytes/macrophages (34, 47, 48). Conversely, P2ry12$^+$ microglia were Cx3cr1-GFP$^+$ (Fig. 6*C*).

Because microglia were in direct contact with CD11b$^+$ infiltrating macrophages, it is possible that microglia affect the activity and/or infiltration of macrophages. To examine this possibility, we depleted microglia and evaluated CD11b$^+$ cells in whole-mount retinas 24 h post-RD. Interestingly, in detached retinas from microglia-depleted TG mice, infiltration of CD11b$^+$ macrophages was markedly suppressed compared with retinas from control mice ($P < 0.01$) (Fig. 7 *A* and *B* and *SI Appendix*, Fig. S11*B*). Moreover, CD11b$^+$ macrophages were almost absent in detached retinas from PLX5622-fed C57BL/6J mice ($P < 0.01$) (Fig. 7 *C* and *D* and *SI Appendix*, Fig. S11*C*). The absence of microglia and CD11b$^+$ cells in PLX5622-treated RD retinas was also confirmed in cross-sectional analysis (Fig. 7*E*). It should be noted that some CD11b$^+$ macrophages were observed in the far peripheral retina around the RD injection site in both microglia depletion methods, indicating that the systemic CD11b$^+$ macrophage population was not significantly decreased by microglia depletion methods (*SI Appendix*, Fig. S11). In addition, we confirmed by flow cytometric analysis that the systemic (blood and spleen) CD11b$^+$ cell populations did not change significantly with either microglia depletion method (*SI Appendix*, Fig. S12). These results suggest that loss of microglia is the direct cause of reduced infiltrating CD11b$^+$ macrophages in the retina, indicating that microglia control the infiltration of macrophages into the damaged tissue.

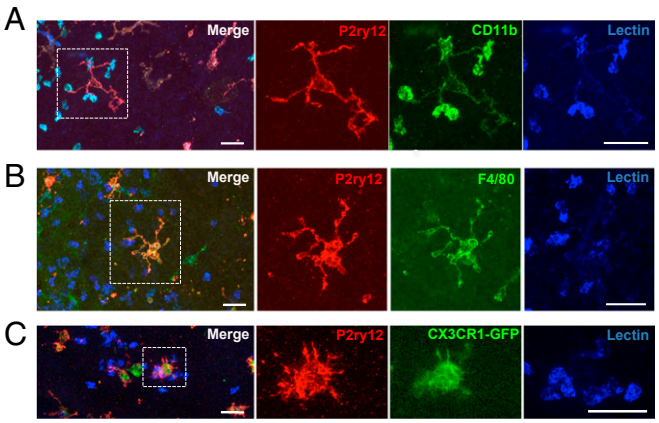

Fig. 6. Infiltrating cells 24 h post-RD are CD11b$^+$, F4/80$^-$, and CX3CR1$^-$. Retinas 24 h post-RD were stained with anti-P2ry12 Ab and lectin together with anti-CD11b Ab (*A*) or anti-F4/80 Ab (*B*), or CX3CR1$^+$/GFP mice were used (*C*). Images around the peak of RD were taken by confocal microscopy using a 63× lens. Z-stack images of the bottom of the retinas were created by ImageJ. Magnified single-color images of the microglia indicated by dotted squares are shown on the *Right*. Lectin$^+$ cells interacted by microglia are CD11b$^+$, F4/80$^-$, and CX3CR1-GFP$^-$. At least three eyes were examined for each staining. (Scale bars: 25 μm.)

Downloaded at Palestinian Territory, occupied on December 1, 2021

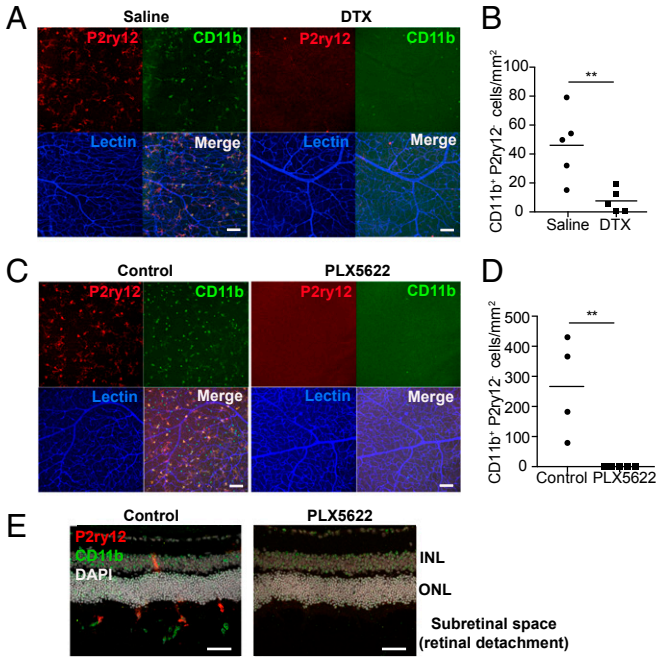

Fig. 7. $CD11b^{+}P2ry12^{-}$ macrophage infiltration is decreased in association with microglia depletion. The eyes were isolated 24 h post-RD with or without microglia depletion. (*A*–*D*) Whole-mount retinas were stained for P2ry12, CD11b, and lectin. (*A* and *C*) Z-stack images of the center of the detached area, which corresponds to the peak of RD, were obtained by confocal microscopy using a 63× lens. Consequently, two images were obtained per eye. (*B* and *D*) The number of $CD11b^{+}P2ry12^{-}$ cells in the photoreceptor layer was manually counted using z-stack images created by ImageJ. The results from two images from the same eye were averaged and shown as the cell number from the eye (*B*, $n = 5$; *D*, $n = 4$–5). (*A* and *B*) Microglia depletion in TG mice (CX3CR1cre × B6-iDTR). DTX or saline was AC inoculated in TG mice 48 h before and at the time of RD surgery. (*C* and *D*) Microglia depletion with PLX5622. PLX5622 or control diet was given starting 7 d before RD induction in C57BL/6J mice. (*E*) Fresh-frozen eyes preserved in OCT compound were stained for P2ry12, CD11b, and DAPI. Representative images from at least 12 sections from three eyes per group are presented. (Scale bars: 100 μm in *A* and *C*; 50 μm in *E*.) Data are expressed as mean; $^{**}P < 0.01$, unpaired *t* test.

Microglial Phagocytosis of Autofluorescent Particles in the Photoreceptor Layer. We have shown that microglia and inflammatory cells migrate rapidly into the photoreceptor layer within 24 h in RD. These observations suggest that in the early stage of RD the primary immune cell activity occurs in the photoreceptor layer, which is the location of retinal injury in this model. We have shown that microglia at this stage interact with $CD11b^{+}$ macrophages, although there were also numerous amoeboid microglia that did not have contact with $CD11b^{+}$ macrophages but were located within the photoreceptor layer. This suggests that activated microglial subsets may perform differing functions in the damaged photoreceptor layer.

Previous studies have demonstrated that when microglia/macrophages engulf damaged photoreceptors, the engulfed photoreceptors can be identified by autofluorescence within phagocytic vacuoles (49, 50). We examined if autofluorescence was detected in amoeboid microglia within the damaged photoreceptor layer in mice with RD. Retinas of 24 h post-RD mice were stained with anti-P2ry12 Ab, and confocal images around the center of the detachment were taken together with autofluorescence identified at the 488-nm excitation wavelength (50, 51). Interestingly, autofluorescence was observed within the cell bodies of amoeboid microglia (Fig. 8*A*), indicating phagocytosis of injured photoreceptors. Magnified 3D-reconstructed images clearly show that the microglia cell bodies contain multiple autofluorescent particles approximately 2–3 μm in diameter (Fig. 8*B*). While $CD11b^{+}$ macrophages also contain autofluorescence in their cell bodies (Fig. 8*C*), the average autofluorescent volume within a single microglial cell body was seven times larger than that in a single macrophage, and the total area of autofluorescence in all microglia was five times larger than that of macrophages (Fig. 8*D*). This suggests

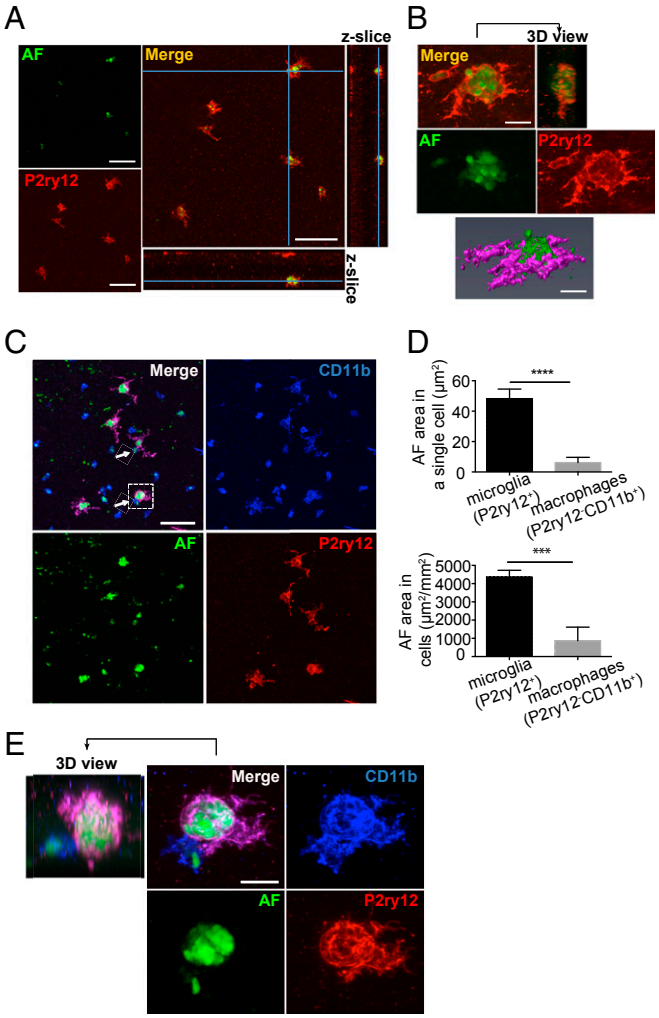

Fig. 8. Phagocytosis of autofluorescent particles by activated microglia. Whole-mount retinas 24 h post-RD were stained with P2ry12 and CD11b. Confocal images were taken together with autofluorescence excited at 488 nm. (*A* and *B*) Representative images of four retinas. (*A*) Single-slice images and orthogonal z-slices of microglia and autofluorescence in the outer retina created by ImageJ. Microglia cell bodies and autofluorescence colocalize. (*B*) Z-stack images and a 3D-constructed image of a microglia phagocytizing autofluorescent particles created by ImageJ and Amira. The microglia contains multiple autofluorescent particles in its cell body. (*C*) Z-stack images of the bottom of the retina. Microglia ($P2ry12^{+}$) and macrophages ($P2ry12^{-}CD11b^{+}$) contain autofluorescence in their cell bodies. Microglia interacting with macrophages are indicated by arrows. (*D*) Evaluation of the autofluorescence area in a single cell (*Upper*) and in a 1-mm^2 area (*Lower*). Four confocal images (each area 246.03 × 246.03 μm) were taken per retina. All the $P2ry12^{+}$ microglia (20–27 cells per retina) and $P2ry12^{-}CD11b^{+}$ macrophages (10–49 cells per retina) which contain autofluorescence in the four images per retina were evaluated to calculate the area of autofluorescence (AF). $^{***}P < 0.001$; $^{****}P < 0.0001$. (*E*) Magnified images of a single microglia indicated by the dashed square in *C*. A microglia containing autofluorescence interacts with a macrophage. A 360° video image of this microglia is shown in Movie S4. (*C*–*E*) $n = 4$ retinas (16 images). (Scale bars: 50 μm in *A*; 10 μm in *B*; 50 μm in *C*; 10 μm in *E*.)

Downloaded at Palestinian Territory, occupied on December 1, 2021

that microglia are the main cell population contributing to phagocytosis of damaged photoreceptors. Some of the autofluorescence-containing microglia also interacted with CD11b$^+$ macrophages (Fig. 8*E* and Movie S4), indicating that microglia may have diverse functions depending on disease pathology. The association of microglia, autofluorescence, and CD11b$^+$ macrophages was also examined by IHC in retinal cross-sections. Amoeboid microglia containing autofluorescence adjacent to the ONL were observed interacting with CD11b$^+$ macrophages in the subretinal space (*SI Appendix*, Fig. S13). Moreover a number of microglia entering the subretinal space were also identified (*SI Appendix*, Fig. S13*B*), suggesting some of the activated microglia may exit the retina during RD. These data demonstrate that following injury there is dynamic microglial phagocytic activity in the photoreceptor layer, which may protect surrounding photoreceptors from further damage. Thus, an important function of microglia following RD is clearing distressed or dying photoreceptors.

Discussion

In this study we demonstrated that in response to RD microglia undergo dramatic morphological changes following activation. Activated microglia traveled rapidly into the damaged photoreceptor layer within 24 h post-RD, where microglia either interact with infiltrating macrophages and/or engulf dying photoreceptors.

In the present study, we observed microglial activation within as little as 1 h after RD induction. This microglia activation started earlier than the peak of photoreceptor cell death, which occurs at 24 h in this RD model (13, 52). At 24 h post-RD, activated microglia were located in the photoreceptor layer, indicating that the target of activated microglia in RD is the photoreceptor layer, where direct injury occurs. It should be noted that microglia with multiple different morphologies (fully amoeboid and ramified) exist in the outer retina at 24 h post-RD (Fig. 5). Some microglia even remained in the inner retina after RD (*SI Appendix*, Figs. S3 and S9), and microglia migrating into the subretinal space were observed (*SI Appendix*, Fig. S13*B*). This suggests that microglia are not a homogenous population but rather contain several subsets with discrete functions, as recently demonstrated in brain-resident Fcrls$^+$ microglia that contained three distinct populations with different cytokine expression patterns (53).

We observed that the loss of retinal microglia resulted in increased photoreceptor cell death in response to RD, suggesting that retinal microglia have a role in inhibiting photoreceptor cell death in this acute injury model. While ERG analysis did not detect any change in retinal function in microglia-depleted RD retinas, this could be due to the limitations of the ERG technology in detecting retinal changes in the detached retina. In human RD, full-field ERG recordings from patients with total RD have an almost nonrecordable ERG response which is not predictive of retinal function after reattachment (45). In our murine RD model, RD is induced in approximately 50% of the total retinal area (6). The results of a full-field ERG include both the nondetached area and detached area, although very little signal is likely to originate from the detached area. This indicates that the ERG recordings obtained in this murine RD model originate predominately from nondetached areas and that the amplitudes would be reflective of the size/function of the nondetached retina, not the area of detachment. Although many reports demonstrate photoreceptor cell death in murine models of sodium hyaluronate-induced RD, ERG data were not presented in these reports (11, 54–57).

There are reports of ERG differences in saline-injected surgical murine RD models (58, 59). Saline is rapidly absorbed, and reattachment occurs within 1–3 d after injection (60). Therefore, ERG recordings of saline-injected retinas are reflective of both the reattached retina and the nondetached retina. By contrast, injection of sodium hyaluronate, which we used in the present study, induces persistent and stable RD, preventing ERG assessment.

We have identified that one function of microglia in RD is to phagocytose injured photoreceptors, as detected by the autofluorescent signature in microglia (Fig. 8). It is generally known that autofluorescent material, called "lipofuscin," originates from the ingestion of shed photoreceptor outer segments. The outer segments are renewed approximately every 10–14 d in normal conditions, and outer segments that are shed from the photoreceptor cell bodies are normally phagocytized by RPE cells (61). Conventionally, lipofuscin in RPE cells is known as the main source of fundus autofluorescence, although perivascular and subretinal microglia/macrophages have also been shown to be an important source of autofluorescence in the aged retina (51). It is thought that the accumulation of lipofuscin is one of the causes of increased photoreceptor cell death in mouse models of accelerated senescence (62) and Stargardt disease (63). In disease conditions, microglia and/or macrophages will phagocytize degraded outer segments and become a source of autofluorescence in the injured area (50, 64, 65). However, due to the absence of specific markers for microglia and macrophages, the identity of cell populations containing autofluorescence was not clear in previous studies (49, 64). In the current report, using a microglia-specific anti-P2ry12 antibody (35), we clearly demonstrate that microglia contain autofluorescence in RD. These results suggest that microglia may contribute to maintaining a homeostatic microenvironment by removing injured photoreceptor outer segments. While we observed autofluorescence in macrophages, this autofluorescence was minimal in volume compared with microglia, suggesting that microglia play a more significant role in photoreceptor removal.

We also observed that activated microglia interacted with CD11b$^+$ macrophages, which have a morphology and staining pattern different from that of microglia. Interestingly, infiltration of CD11b$^+$ macrophages, which was prominent in the control mice at 24 h post-RD, was suppressed in retinas from microglia-depleted mice (Fig. 7). This could be explained by one of two scenarios.

First, CX3CR1$^+$ cell depletion by DTX and CSF1R blockade by PLX5622 might have depleted systemic CD11b$^+$ macrophage populations as well. CSF1R is also expressed in blood monocytes and is important for the survival, maturation, and differentiation of these cells (66, 67), and therefore it is possible that PLX5622 suppressed systemic CD11b$^+$ monocytes as well. Likewise, although DTX was administered locally in the eye in the TG model, it could potentially enter the circulation and deplete systemic monocytes. However, we demonstrated that neither microglia depletion method changed the relative levels of circulating CD11b$^+$ cell populations (*SI Appendix*, Fig. S12). A prior study demonstrating that PLX5622 does not alter circulating monocyte numbers (68) supports our results.

The second possibility is that in the absence of microglia, CD11b$^+$ cellular infiltration into the retina is blocked. Microglia may direct infiltrating cells from the systemic circulation into the retina during injury, and in the absence of microglia immune cells are blocked from CNS entry. No previous studies have identified that microglia direct the CNS immune response, and this newly discovered interaction could be of significant interest as a therapeutic target. This finding also suggests heterogeneity in microglial function in RD, as microglia both direct the immune response in early phases of RD and later engulf immune cells. It seems likely that distinct subpopulations of microglia may perform these discrete functions and keep neuroinflammation in check.

We are just beginning to understand the roles of retinal microglia in response to the acute injury of RD. Our current study demonstrates that the absence of microglia exacerbates photoreceptor cell death along with a corresponding reduction of CD11b$^+$ cells infiltrating into the injured retina in RD (Figs. 3, 4, and 7). The association of infiltrating macrophages with photoreceptor cell death remains controversial. Our previous findings suggested that inflammatory cytokines, such as IL-1β, MCP-1, and TNF-α produced by CD11b$^+$ macrophages/microglia may increase

Downloaded at Palestinian Territory, occupied on December 1, 2021

photoreceptor cell death (13). We therefore expected photoreceptor cell death to be reduced in microglia-depleted retinas, as this decreased both microglia and macrophages (Fig. 7). Surprisingly, photoreceptor cell death was increased in microglia-depleted retinas (Figs. 3 and 4). It is known that microglia produce trophic factors such as brain-derived neurotrophic factor (24) and that Müller cells increase the expression of trophic factors when they are cocultured with activated microglia (69). Further, these trophic factors produced by microglia and Müller cells increased photoreceptor viability in vitro (69). It is also likely that distinct populations of microglia may have differential effects on photoreceptor survival. In addition, damaged photoreceptors that are not phagocytized in microglia-depleted retinas may trigger apoptosis of neighboring photoreceptors, resulting in an expansion of damaged tissue. It is likely that the effect of microglial depletion on photoreceptor cell death is multifactorial.

Although the present study yields important insights into the function of microglia in retinal injury, it is important to recognize the inherent and unavoidable limitations. First, there are differences between human RD and animal models of RD. In animal models, RD is created surgically within a few minutes, which would be similar to traumatic RD in human patients (6, 23). However, the mechanism of photoreceptor damage may differ when RD is triggered not by traumatic injury but as a consequence of retinal disease in which RD forms gradually over time. Because RD occurs as a complication of many retinal diseases, it is possible that microglia have differential functions dependent on the underlying cause of RD. Second, we use sodium hyaluronate (1%), which is highly viscous, to create a stable RD in animals. By contrast, the subretinal fluid in human RD is primarily liquefied vitreous, serum transudate, and aqueous humor (70, 71). Sodium hyaluronate is the predominant glycosaminoglycan of human vitreous, and the concentration of hyaluronan in adult human vitreous has reported to be between approximately 0.0065 and 0.04% (72), much lower than the concentration used for induction of RD in animals. However, despite these differences, there are multiple similarities between animal RD models and human RD, such as activation of IL-1β (13), subretinal microglia/macrophage infiltration (65), and timing of apoptotic cells observed in the ONL (4). Third, although P2ry12 is expressed exclusively in microglia, P2ry12 expression has been reported to be decreased in some disease conditions (73, 74). Therefore, it is possible that, post- RD, some activated microglia down-regulate P2ry12 expression, although activated P2ry12^{+} amoeboid microglia were observed in the photoreceptor layer (Figs. 2, 5, 7, and 8) and in the subretinal space (*SI Appendix*, Fig. S13*B*).

In summary, our results indicate that in acute RD microglia help maintain photoreceptor viability and protect photoreceptor cells from degeneration, in part via microglia-mediated control of macrophage infiltration and photoreceptor phagocytosis.

Materials and Methods

Animals. All animal experiments followed the guidelines of the Association for Research in Vision and Ophthalmology Statement for the Use of Animals in Ophthalmic and Vision Research and were approved by the Animal Care Committee of the Massachusetts Eye and Ear Infirmary. C57BL/6J mice (stock no. 00664) and CX3CR1$^{GFP/GFP}$ mice on a C57BL/6 background (stock no. 005582), *Cx3cr1*^{CreER} mice (stock no. 021160), and B6-iDTR mice (stock no. 007900) were purchased from Jackson Laboratories. Heterozygous CX3CR1$^{+/GFP}$ mice were created by crossing CX3CR1$^{GFP/GFP}$ mice with wild-type C57BL/6J mice. Mice were fed standard laboratory chow except during the microglia-depletion experiments, in which PLX5622 or the control diet was given. Mice were allowed free access to water in a climate-controlled room with a 12-h light/12-h dark cycle. All mice used for experiments were 7–9 wk old.

Induction of RD. RD was induced as previously described (6). Briefly, mice were anesthetized with an i.p. injection of 2,2,2-tribromoethanol (250 mg/kg; Sigma-Aldrich Corp.), and pupils were dilated with topical phenylephrine (5%) and tropicamide (0.5%). The temporal conjunctiva at the posterior limbus was incised and detached from the sclera. A 30-gauge needle (BD) was used with the bevel pointed up to create a sclerotomy 1 mm posterior to the limbus. A scleral tunnel was created, followed by scleral penetration into the choroid, making a self-sealing scleral wound. A corneal puncture was made with a 30-gauge needle to lower intraocular pressure. A 33-gauge needle connected to a NanoFil 10-μL syringe (World Precision Instruments, Inc.) was inserted into the subretinal space with the bevel pointed down. Then, 4 μL of 1% sodium hyaluronate (Provisc; Alcon) was gently injected, detaching approximately 60% of the temporal-nasal neurosensory retina from the underlying RPE. Finally, cyanoacrylate surgical glue (Webglue; Patterson Veterinary) was applied to the scleral wound, and the conjunctiva was reattached to the original position. Eyes with subretinal hemorrhage or unsuccessful detachment were excluded from analysis.

Microglia Depletion. Microglia depletion was performed using *Cx3cr1*^{CreER} × B6-iDTR (TG) mice or PLX5622 (Plexxikon Inc.), an orally available, selective CSF1R inhibitor incorporated into rodent chow. To generate TG mice, *Cx3cr1*^{CreER} mice, which express Cre-ER fusion protein from endogenous CX3CR1 promoter enhance elements (40), were crossed with B6-iDTR mice, which contain a flox-STOP-flox DTR in the ROSA26 locus (41). In this TG mouse system, Cre recombinase activation under control of the *Cx3cr1* promoter can be induced by tamoxifen, which leads to surface expression of DTR on CX3CR1-expressing cells. The activation of Cre recombinase was induced by five consecutive days of i.p. tamoxifen injection (Sigma-Aldrich) (2 mg per mouse per day) at age 6 wk. Tamoxifen was dissolved in corn oil (Sigma-Aldrich) at a final concentration of 20 mg/mL. The suspension was heated at 50 °C until dissolved. At age 8 wk, DTX (Sigma-Aldrich) (25 ng/1 μL saline) AC inoculation was conducted to deplete CX3CR1-expressing cells following a previous report (42). DTX AC administration was performed 2 d before and right after RD induction. Control mice were given saline (AC).

For microglia depletion using PLX5622, mice were fed the control chow (AIN-76) or chow containing 1,200 ppm of PLX5622 1 wk before RD induction. No obvious behavioral or health problems were observed as a result of the PLX5622-supplemented diet.

IHC of Whole-Mount Retinas. After anesthesia, eyes were enucleated following retinal perfusion with PBS. The eyes were fixed in 4% paraformaldehyde (PFA) in 2× PBS for 15 min and then were transferred to 2× PBS on ice for 10 min. After the eyes were dissected, retinal whole mounts were prepared. The detached area was easily distinguishable by the characteristic morphology. The retinas were then transferred to ice-cold methanol and kept at −80 °C until use. For IHC, rabbit anti-P2ry12 Ab (1:500; a gift from H.L.W.), rat anti-CD11b Ab (1:100, clone M1/70; Abcam), and rat anti-F4/80 Ab (1:2,000, clone CI:A3-1; Bio-Rad) were used for primary antibodies, and Alexa Fluor 594-conjugated goat anti-rabbit Ab and Alexa Fluor 488-conjugated goat anti-rat Ab (1:500; Thermo Fisher Scientific) were used for secondary antibodies. The retinas were first blocked in a blocking buffer (0.3% Triton X-100, 0.2% BSA, and 5% goat serum in PBS) for 1 h at room temperature and were incubated with primary antibodies and Alexa Fluor 647-conjugated Isolectin GS-B4 (1:100; Thermo Fisher Scientific) overnight at 4 °C. After washing, the retinas were incubated with secondary antibodies for 4 h at 4 °C. The retinas were mounted after washing.

Image Processing and Analysis. Images of whole-mount retinas and cross-sections were captured by confocal microscopy (SP5 or SP8; Leica) or epifluorescent microscopy (Axio Observer Z1; Carl Zeiss). For autofluorescence detection, the laser was excited at 488 nm, and emission at 500–600 nm was detected. For confocal images of detached retinas, images were taken around the center of each bump of the detached area. For evaluation of microglial cell number and density, one image (775 × 775 μm) from each detached area was taken. Therefore, images of two fields were obtained from each flat-mounted retina with detachment. For quantification of the autofluorescence area, four images (each 246.03 × 246.03 μm) were taken per retina. The images processed by ImageJ (NIH) were used. For microglial cell number counting, microglial cell bodies were counted manually based on the z-stack images. For microglial density evaluation, maximum intensity z-stack images were created, and the images were processed with the smoothing, make binary, and watershed tools. The area of particles was then calculated using the analyze particles tool, setting the size range to 10–1,000. For evaluation of the autofluorescence area, maximum intensity z-stack images were created, and the areas of autofluorescence were segmented using the threshold tool. The segmented areas were measured using the analyze particles tool, setting the size range at 1–1,000. Amira 5 software (FEI) was used to make 3D-reconstruction images. The numbers of P2ry12^{-}CD11b^{+} cells were counted manually using enlarged z-stack images

Downloaded at Palestinian Territory, occupied on December 1, 2021

and single-scan images from each series scan to clearly distinguish P2ry12$^-$ CD11b$^+$ cells from autofluorescence and P2r12$^+$CD11b$^+$ double-positive cells.

TUNEL Staining. TUNEL staining for RD was performed as previously described (52). RD eyes were enucleated and embedded in OCT compound (Tissue-Tek; Sakura Finetek). Serial sections in the sagittal plane were cut at 10-μm thickness on a cryostat (CM1950; Leica). Sections approximately 1,000 μm from the injection site, which is the region of the most significant RD, were used for disease assessment (*SI Appendix*, Fig. S14). The TUNEL assay was performed according to the manufacturer's protocol (In Situ Cell Death Detection Kit, TMR red; Roche), and cell nuclei were stained with DAPI (Vectashield; Vector). Images of the center of detachment were taken by epifluorescence microscopy (Axio Observer Z1) using a 40× lens. The areas imaged for TUNEL evaluation are theoretically a stable distance from the optic disk and are at the same location within each detached retina (*SI Appendix*, Fig. S14). TUNEL$^+$ cells in the ONL, containing the photoreceptor cell bodies, were counted manually. The area of the ONL was also measured by ImageJ, and TUNEL$^+$ cell density in the ONL was calculated. The average TUNEL$^+$ cell density at two parts of the retina was calculated as the representative TUNEL$^+$ photoreceptor cell density of the section. Then, the average of the TUNEL$^+$ photoreceptor cell densities from four sections was determined as the representative TUNEL$^+$ photoreceptor cell density of the eye. The ONL thickness was measured manually using ImageJ in the images used for TUNEL evaluation. The ONL thickness at three points per section was measured to calculate the thickness of the section (12).

IHC for Cross-Sections. For costaining with TUNEL, fixed eyes were used for IHC. After anesthesia, the animals were perfused with PBS and 4% PFA. The eyes were fixed in 4% PFA for 1 h and were treated in 10%, 20%, and 30% sucrose-PBS for 1 h each. The eyes were embedded in OCT compound. Serial sections in the sagittal plane were cut at a 20-μm thickness on a cryostat. IHC was performed after TUNEL staining (ApopTag; Millipore). For IHC with fresh-frozen eyes, 10-μm-thick sections were used. Rabbit anti-recoverin Ab (1:100; Millipore), anti-P2Y12 Ab (1:500–1:10,000; AnaSpec), and anti-CD11b (1:100) were used for primary Abs (overnight at 4 °C), and sections were incubated with secondary antibodies for 1 h at room temperature. The sections were finally stained with DAPI (300 nM; Thermo Fisher Scientific), and images were taken by confocal microscopy (SP8; Leica).

ERG Recording. Full-field ERGs were recorded after dark adaptation overnight (>12 h). Mice were anesthetized with i.p. injections of a mixture of ketamine (90 mg/kg) and xylazine (9 mg/kg). Mydriasis was achieved with one drop of 0.5% tropicamide with 5% phenylephrine. Corneal anesthesia was performed with a single drop of 0.5% proparacaine hydrochloride ophthalmic solution (Akorn Inc.). A warm heating pad was used to maintain body temperature (37 °C). ERGs were recorded using the HMsERG LAB system (OcuScience). Stimulus flashes were presented in a Ganzfeld bowl. Stimulus intensities ranging from −1.5 to 1.0 log cd s/m^2 in 0.5-log unit steps were used under dark-adapted conditions. Light stimuli were presented with a 1-min interval between successive stimuli.

Flow Cytometric Analysis. For CD11b$^+$ cell evaluation from animals with microglia depletion, microglia depletion was performed using Cx3cr1CreER × B6-iDTR (TG) mice or chow containing the CSF1R antagonist PLX5622. In TG mice, all the animals received i.p. injections of tamoxifen (2 mg per mouse per day) for five consecutive days. Two weeks later, 1 μL of vehicle (saline) or DTX (25 ng/1 μL saline) was injected in the AC 3 d and 1 d before the experiment, following the procedure performed for microglia depletion in RD. C57BL/6 mice were started on PLX5622 or control chow 7 d before the experiment. On the day of the experiment, approximately 1 mL of blood was obtained from each animal by cardiac puncture. Blood samples were collected in a tube containing EDTA, and lymphocytes were collected by gradient centrifugation using Hitopaque-1083 solution (Sigma-Aldrich). Spleens were harvested, and single-cell suspensions were prepared. The cells were stained with CD45-FITC (30-F11; BD Bioscience) and CD11b-PECy7 (M1/70; BioLegend).

For flow cytometric analysis of microglia in RD, mice were perfused with PBS, and retinas were collected from control animals and RD animals 12 h and 24 h post-RD. Ten retinas per group were pooled and gently homogenized in HBSS using a glass tissue homogenizer. Single-cell suspensions were prepared and centrifuged over a 37%/70% discontinuous Percoll gradient (GE Healthcare), and mononuclear cells were isolated from the interface. Isolated cells were labeled with FRCLS antibody to specifically identify resident microglia (35).

The samples were examined on an LSR II flow cytometer (BD Bioscience) in the presence of DAPI. Acquired data were analyzed using FlowJo 10.1.

Statistical Analysis. Data are presented as the mean ± SEM. Differences between two groups were analyzed using an unpaired two-tailed Student's *t* test. Multiple-group comparisons were performed by one-way ANOVA followed by Tukey's multiple comparison test. All statistical analysis was performed using GraphPad software (Prism 6; GraphPad Software, Inc.). Significance levels are marked $*P < 0.05$; $**P < 0.01$; $***P < 0.001$; and $****P < 0.0001$ in figures.

ACKNOWLEDGMENTS. We thank Plexxikon Inc. for providing PLX5622 chow and M. Saint-Geniez (Schepens Eye Research Institute) for ERG analysis advice. This study was supported by NIH/National Eye Institute Grant R01EY027303 (to K.M.C.); the Massachusetts Lions Eye Research Fund (K.M.C.); Global Ophthalmology Awards Program Research Award by Bayer in 2016 (to Y.O.); and a Research to Prevent Blindness unrestricted grant (to J.W.M.). K.M.C. was supported by the Department of Ophthalmology, Harvard University, and Massachusetts Eye and Ear Infirmary.

1. Rowe JA, et al. (1999) Retinal detachment in Olmsted county, Minnesota, 1976 through 1995. *Ophthalmology* 106:154–159.
2. Bird AC, et al.; The International ARM Epidemiological Study Group (1995) An international classification and grading system for age-related maculopathy and age-related macular degeneration. *Surv Ophthalmol* 39:367–374.
3. Aiello LM (2003) Perspectives on diabetic retinopathy. *Am J Ophthalmol* 136:122–135.
4. Arroyo JG, Yang L, Bula D, Chen DF (2005) Photoreceptor apoptosis in human retinal detachment. *Am J Ophthalmol* 139:605–610.
5. van Bussel EM, van der Valk R, Bijlsma WR, La Heij EC (2014) Impact of duration of macula-off retinal detachment on visual outcome: A systematic review and meta-analysis of literature. *Retina* 34:1917–1925.
6. Matsumoto H, Miller JW, Vavvas DG (2013) Retinal detachment model in rodents by subretinal injection of sodium hyaluronate. *J Vis Exp*, 10.3791/50660, and erratum (2014), 10.3791/5138.
7. Zacks DN, Han Y, Zeng Y, Swaroop A (2006) Activation of signaling pathways and stress-response genes in an experimental model of retinal detachment. *Invest Ophthalmol Vis Sci* 47:1691–1695.
8. Yu J, Peng R, Chen H, Cui C, Ba J (2012) Elucidation of the pathogenic mechanism of rhegmatogenous retinal detachment with proliferative vitreoretinopathy by proteomic analysis. *Invest Ophthalmol Vis Sci* 53:8146–8153.
9. Matsumoto H, et al. (2014) Mammalian STE20-like kinase 2, not kinase 1, mediates photoreceptor cell death during retinal detachment. *Cell Death Dis* 5:e1269.
10. Nakazawa T, et al. (2006) Characterization of cytokine responses to retinal detachment in rats. *Mol Vis* 12:867–878.
11. Nakazawa T, et al. (2007) Monocyte chemoattractant protein 1 mediates retinal detachment-induced photoreceptor apoptosis. *Proc Natl Acad Sci USA* 104:2425–2430.
12. Nakazawa T, et al. (2011) Tumor necrosis factor-alpha mediates photoreceptor death in a rodent model of retinal detachment. *Invest Ophthalmol Vis Sci* 52:1384–1391.
13. Kataoka K, et al. (2015) Macrophage- and RIP3-dependent inflammasome activation exacerbates retinal detachment-induced photoreceptor cell death. *Cell Death Dis* 6:e1731.
14. Ginhoux F, et al. (2010) Fate mapping analysis reveals that adult microglia derive from primitive macrophages. *Science* 330:841–845.
15. Cebulla CM, et al. (2012) A chick model of retinal detachment: Cone rich and novel. *PLoS One* 7:e44257.
16. Lam TT, Kwong JM, Tso MO (2003) Early glial responses after acute elevated intraocular pressure in rats. *Invest Ophthalmol Vis Sci* 44:638–645.
17. Gupta N, Brown KE, Milam AH (2003) Activated microglia in human retinitis pigmentosa, late-onset retinal degeneration, and age-related macular degeneration. *Exp Eye Res* 76:463–471.
18. Penfold PL, Madigan MC, Gillies MC, Provis JM (2001) Immunological and aetiological aspects of macular degeneration. *Prog Retin Eye Res* 20:385–414.
19. Zeng HY, Green WR, Tso MO (2008) Microglial activation in human diabetic retinopathy. *Arch Ophthalmol* 126:227–232.
20. Zhao L, Ma W, Fariss RN, Wong WT (2009) Retinal vascular repair and neovascularization are not dependent on CX3CR1 signaling in a model of ischemic retinopathy. *Exp Eye Res* 88:1004–1013.
21. Connor KM, et al. (2007) Increased dietary intake of omega-3-polyunsaturated fatty acids reduces pathological retinal angiogenesis. *Nat Med* 13:868–873.
22. Fischer AJ, Zelinka C, Milani-Nejad N (2015) Reactive retinal microglia, neuronal survival, and the formation of retinal folds and detachments. *Glia* 63:313–327.
23. Lewis GP, Sethi CS, Carter KM, Charteris DG, Fisher SK (2005) Microglial cell activation following retinal detachment: A comparison between species. *Mol Vis* 11:491–500.
24. Karlstetter M, et al. (2015) Retinal microglia: Just bystander or target for therapy? *Prog Retin Eye Res* 45:30–57.
25. Karlstetter M, Ebert S, Langmann T (2010) Microglia in the healthy and degenerating retina: Insights from novel mouse models. *Immunobiology* 215:685–691.

Downloaded at Palestinian Territory, occupied on December 1, 2021

26. Peng B, et al. (2014) Suppression of microglial activation is neuroprotective in a mouse model of human retinitis pigmentosa. *J Neurosci* 34:8139–8150.
27. Hanafy KA (2013) The role of microglia and the TLR4 pathway in neuronal apoptosis and vasospasm after subarachnoid hemorrhage. *J Neuroinflammation* 10:83.
28. Sokolowski JD, Chabanon-Hicks CN, Han CZ, Heffron DS, Mandell JW (2014) Fractalkine is a "find-me" signal released by neurons undergoing ethanol-induced apoptosis. *Front Cell Neurosci* 8:360.
29. Zhao L, et al. (2015) Microglial phagocytosis of living photoreceptors contributes to inherited retinal degeneration. *EMBO Mol Med* 7:1179–1197.
30. Neumann J, et al. (2008) Microglia cells protect neurons by direct engulfment of invading neutrophil granulocytes: A new mechanism of CNS immune privilege. *J Neurosci* 28:5965–5975.
31. Kawabori M, et al. (2015) Triggering receptor expressed on myeloid cells 2 (TREM2) deficiency attenuates phagocytic activities of microglia and exacerbates ischemic damage in experimental stroke. *J Neurosci* 35:3384–3396.
32. Huang H, Parlier R, Shen JK, Lutty GA, Vinores SA (2013) VEGF receptor blockade markedly reduces retinal microglia/macrophage infiltration into laser-induced CNV. *PLoS One* 8:e71808.
33. Wang M, et al. (2014) Macroglia-microglia interactions via TSPO signaling regulates microglial activation in the mouse retina. *J Neurosci* 34:3793–3806.
34. Rangasamy S, et al. (2014) Chemokine mediated monocyte trafficking into the retina: Role of inflammation in alteration of the blood-retinal barrier in diabetic retinopathy. *PLoS One* 9:e108508.
35. Butovsky O, et al. (2014) Identification of a unique TGF-β-dependent molecular and functional signature in microglia. *Nat Neurosci* 17:131–143.
36. Salter MW, Beggs S (2014) Sublime microglia: Expanding roles for the guardians of the CNS. *Cell* 158:15–24.
37. Haynes SE, et al. (2006) The P2Y12 receptor regulates microglial activation by extracellular nucleotides. *Nat Neurosci* 9:1512–1519.
38. Hasegawa E, et al. (2014) Characterization of a spontaneous retinal neovascular mouse model. *PLoS One* 9:e106507.
39. Fernández-Arjona MDM, Grondona JM, Granados-Durán P, Fernández-Llebrez P, López-Ávalos MD (2017) Microglia morphological categorization in a rat model of neuroinflammation by hierarchical cluster and principal components analysis. *Front Cell Neurosci* 11:235.
40. Parkhurst CN, et al. (2013) Microglia promote learning-dependent synapse formation through brain-derived neurotrophic factor. *Cell* 155:1596–1609.
41. Buch T, et al. (2005) A Cre-inducible diphtheria toxin receptor mediates cell lineage ablation after toxin administration. *Nat Methods* 2:419–426.
42. McPherson SW, Heuss ND, Pierson MJ, Gregerson DS (2014) Retinal antigen-specific regulatory T cells protect against spontaneous and induced autoimmunity and require local dendritic cells. *J Neuroinflammation* 11:205.
43. Ishihara Y, Itoh K, Ishida A, Yamazaki T (2015) Selective estrogen-receptor modulators suppress microglial activation and neuronal cell death via an estrogen receptor-dependent pathway. *J Steroid Biochem Mol Biol* 145:85–93.
44. Elmore MR, et al. (2014) Colony-stimulating factor 1 receptor signaling is necessary for microglia viability, unmasking a microglia progenitor cell in the adult brain. *Neuron* 82:380–397.
45. Azarmina M, Moradian S, Azarmina H (2013) Electroretinographic changes following retinal reattachment surgery. *J Ophthalmic Vis Res* 8:321–329.
46. Saijo K, Glass CK (2011) Microglial cell origin and phenotypes in health and disease. *Nat Rev Immunol* 11:775–787.
47. Geissmann F, Jung S, Littman DR (2003) Blood monocytes consist of two principal subsets with distinct migratory properties. *Immunity* 19:71–82.
48. Marty S, Dusart I, Peschanski M (1991) Glial changes following an excitotoxic lesion in the CNS–I. Microglia/macrophages. *Neuroscience* 45:529–539.
49. Kim SY, et al. (2014) Deletion of aryl hydrocarbon receptor AHR in mice leads to subretinal accumulation of microglia and RPE atrophy. *Invest Ophthalmol Vis Sci* 55: 6031–6040.
50. Secondi R, Kong J, Blonska AM, Staurenghi G, Sparrow JR (2012) Fundus autofluorescence findings in a mouse model of retinal detachment. *Invest Ophthalmol Vis Sci* 53:5190–5197.
51. Xu H, Chen M, Manivannan A, Lois N, Forrester JV (2008) Age-dependent accumulation of lipofuscin in perivascular and subretinal microglia in experimental mice. *Aging Cell* 7:58–68.
52. Matsumoto H, et al. (2014) Strain difference in photoreceptor cell death after retinal detachment in mice. *Invest Ophthalmol Vis Sci* 55:4165–4174.
53. Ajami B, et al. (2018) Single-cell mass cytometry reveals distinct populations of brain myeloid cells in mouse neuroinflammation and neurodegeneration models. *Nat Neurosci* 21:541–551.
54. Xie J, et al. (2017) Tumor necrosis factor-alpha regulates photoreceptor cell autophagy after retinal detachment. *Sci Rep* 7:17108.
55. Shelby SJ, et al. (2015) Hypoxia inducible factor 1α contributes to regulation of autophagy in retinal detachment. *Exp Eye Res* 137:84–93.
56. Trichonas G, et al. (2010) Receptor interacting protein kinases mediate retinal detachment-induced photoreceptor necrosis and compensate for inhibition of apoptosis. *Proc Natl Acad Sci USA* 107:21695–21700.
57. Chong DY, et al. (2008) Interleukin-6 as a photoreceptor neuroprotectant in an experimental model of retinal detachment. *Invest Ophthalmol Vis Sci* 49:3193–3200.
58. Nour M, Quiambao AB, Peterson WM, Al-Ubaidi MR, Naash MI (2003) P2Y(2) receptor agonist INS37217 enhances functional recovery after detachment caused by subretinal injection in normal and RDS mice. *Invest Ophthalmol Vis Sci* 44:4505–4514.
59. Liu C, et al. (2015) Subretinal injection of amyloid-β peptide accelerates RPE cell senescence and retinal degeneration. *Int J Mol Med* 35:169–176.
60. Qi Y, et al. (2015) Trans-corneal subretinal injection in mice and its effect on the function and morphology of the retina. *PLoS One* 10:e0136523.
61. Bosch E, Horwitz J, Bok D (1993) Phagocytosis of outer segments by retinal pigment epithelium: Phagosome-lysosome interaction. *J Histochem Cytochem* 41:253–263.
62. Sparrow JR, et al. (2012) The bisretinoids of retinal pigment epithelium. *Prog Retin Eye Res* 31:121–135.
63. Wu L, Nagasaki T, Sparrow JR (2010) Photoreceptor cell degeneration in Abcr (-/-) mice. *Adv Exp Med Biol* 664:533–539.
64. Joly S, et al. (2009) Cooperative phagocytes: Resident microglia and bone marrow immigrants remove dead photoreceptors in retinal lesions. *Am J Pathol* 174: 2310–2323.
65. Sekiryu T, Oguchi Y, Arai S, Wada I, Iida T (2011) Autofluorescence of the cells in human subretinal fluid. *Invest Ophthalmol Vis Sci* 52:8534–8541.
66. Chitu V, Stanley ER (2006) Colony-stimulating factor-1 in immunity and inflammation. *Curr Opin Immunol* 18:39–48.
67. Li J, Chen K, Zhu L, Pollard JW (2006) Conditional deletion of the colony stimulating factor-1 receptor (c-fms proto-oncogene) in mice. *Genesis* 44:328–335.
68. Valdearcos M, et al. (2014) Microglia dictate the impact of saturated fat consumption on hypothalamic inflammation and neuronal function. *Cell Rep* 9:2124–2138.
69. Wang M, Ma W, Zhao L, Fariss RN, Wong WT (2011) Adaptive Müller cell responses to microglial activation mediate neuroprotection and coordinate inflammation in the retina. *J Neuroinflammation* 8:173.
70. Smith JL, Douty E (1960) Electrophoresis of subretinal fluid. *Arch Ophthalmol* 64: 114–119.
71. Heath H, Beck TC, Foulds WS (1962) Chemical composition of subretinal fluid. *Br J Ophthalmol* 46:385–396.
72. Grimshaw J, et al. (1994) Quantitative analysis of hyaluronan in vitreous humor using capillary electrophoresis. *Electrophoresis* 15:936–940.
73. Butovsky O, et al. (2015) Targeting miR-155 restores abnormal microglia and attenuates disease in SOD1 mice. *Ann Neurol* 77:75–99.
74. Krasemann S, et al. (2017) The TREM2-APOE pathway drives the transcriptional phenotype of dysfunctional microglia in neurodegenerative diseases. *Immunity* 47: 566–581 e9.

Downloaded at Palestinian Territory, occupied on December 1, 2021